Energy and symmetry of dd excitations in undoped layered cuprates measured by Cu L_3 resonant inelastic x-ray scattering

Energy and symmetry of dd excitations in undoped layered cuprates measured by Cu L_3 resonant inelastic x-ray scattering

M Moretti Sala[1,8,9]**, V Bisogni**[2,10]**, C Aruta**[3]**, G Balestrino**[4]**,
H Berger**[5]**, N B Brookes**[2]**, G M de Luca**[3]**, D Di Castro**[4]**, M Grioni**[5]**,
M Guarise**[5]**, P G Medaglia**[4]**, F Miletto Granozio**[3]**, M Minola**[1]**,
P Perna**[3]**, M Radovic**[3,11]**, M Salluzzo**[3]**, T Schmitt**[6]**, K J Zhou**[6]**,
L Braicovich**[7] **and G Ghiringhelli**[7]

[1] CNISM and Dipartimento di Fisica, Politecnico di Milano,
Piazza Leonardo da Vinci 32, I-20133 Milano, Italy
[2] European Synchrotron Radiation Facility, Boîte Postale 220,
F-38043 Grenoble, France
[3] CNR-SPIN and Dipartimento di Scienze Fisiche, Università di Napoli
'Federico II', Complesso di Monte S Angelo, Via Cinthia, I-80126 Napoli, Italy
[4] CNR-SPIN and Dipartimento di Ingegneria Meccanica, Universitá di Roma
Tor Vergata, Via del Politecnico 1, I-00133 Roma, Italy
[5] Ecole Polytechnique Fédérale de Lausanne (EPFL), Institut de Physique de la
Matiére Condensée, CH-1015 Lausanne, Switzerland
[6] Swiss Light Source, Paul Scherrer Institut, CH-5232 Villigen PSI, Switzerland
[7] CNR-SPIN and Dipartimento di Fisica, Politecnico di Milano,
piazza Leonardo da Vinci 32, I-20133 Milano, Italy
E-mail: marco.moretti@esrf.fr

Abstract. We measured the high-resolution Cu L_3 edge resonant inelastic x-ray scattering (RIXS) of undoped cuprates La_2CuO_4, $Sr_2CuO_2Cl_2$, $CaCuO_2$ and $NdBa_2Cu_3O_6$. The dominant spectral features were assigned to dd excitations and we extensively studied their polarization and scattering geometry

[8] Author to whom any correspondence should be addressed.
[9] Present address: European Synchrotron Radiation Facility, BP 220, F-38043 Grenoble, France.
[10] Present address: IFW Dresden, Postfach 270116, D-01171 Dresden, Germany.
[11] Present address: Swiss Light Source, Paul Scherrer Institut, CH-5232 Villigen PSI, Switzerland.

IOP Institute of Physics Φ DEUTSCHE PHYSIKALISCHE GESELLSCHAFT

dependence. In a pure ionic picture, we calculated the theoretical cross sections for those excitations and used these to fit the experimental data with excellent agreement. By doing so, we were able to determine the energy and symmetry of Cu-3d states for the four systems with unprecedented accuracy and confidence. The values of the effective parameters could be obtained for the single-ion crystal field model but not for a simple two-dimensional cluster model. The firm experimental assessment of dd excitation energies carries important consequences for the physics of high-T_c superconductors. On the one hand, we found that the minimum energy of orbital excitation is always $\geqslant 1.4\,\mathrm{eV}$, i.e. well above the mid-infrared spectral range, which leaves to magnetic excitations (up to $300\,\mathrm{meV}$) a major role in Cooper pairing in cuprates. On the other hand, it has become possible to study quantitatively the effective influence of dd excitations on the superconducting gap in cuprates.

Contents

1. Introduction

Despite the great deal of effort devoted to the study of high-T_c superconductivity in cuprates, a general consensus on the underlying mechanisms is still lacking. It is commonly agreed that low-energy elementary excitations should play a crucial role in the formation of conduction electron Cooper pairs, so that considerable effort is being devoted to establish a link between phonon and magnon spectra and high T_c in cuprates [1–4]. Lattice modes (phonons), which are at the basis of conventional superconductivity as explained by BCS theory, lie below $90\,\mathrm{meV}$, an energy seemingly incompatible with critical temperatures peaking as high as $130\,\mathrm{K}$. And the possible role of spin excitations (magnons) is still debated: the superexchange coupling in layered cuprates is exceptionally large ($J \simeq 130\,\mathrm{meV}$) and gives rise to magnetic excitations up to almost $300\,\mathrm{meV}$. Although in doped superconducting materials the long-range magnetic order is lost, short-range magnetic correlations persist [5], and magnetic excitations survive across the whole reciprocal space as recently shown by Braicovich *et al* [6]. The possible role of magnetic excitations in Cooper pairing has been the subject of several works in the past [7] and is still very actively studied at present [8].

In this context, orbital (dd) excitations, which correspond to a change in the *symmetry* of the occupied Cu-3d orbitals, have attracted much less attention, because their energy is generally much higher (typically > 1.5 eV). However, starting from an advanced use of Eliashberg equations [9], Little *et al* [10] argued that dd excitations are also possibly implicated in the mechanisms of high-T_c superconductivity. Indeed a relation between the Cu to apical-oxygen distance and T_c was found several years ago by Ohta *et al* [11], who proposed a rationale based on Madelung potentials. Ohta *et al* summarized their results in the so-called 'Maekawa plots', reporting the dependence of T_c on the energies needed to transfer the Cu-3d$_{x^2-y^2}$ hole to a Cu-3d$_{3z^2-r^2}$ orbital or to the O-2p states. More recently, Sakakibara *et al* [12] refined the theoretical analysis by a two-orbital model applied to the model structure of La$_{2-x}$Sr$_x$CuO$_4$ and HgBa$_2$CuO$_{4+\delta}$. In their calculations the key parameter is the energy difference between the Cu-3d$_{x^2-y^2}$ and Cu-3d$_{3z^2-r^2}$ states (ΔE_{e_g}): d-wave superconductivity is favored by a larger energy splitting because of the reduced contribution of the d$_{3z^2-r^2}$ state to the Fermi surface. In the mentioned works, the authors based their discussion on theoretically calculated dd excitation energies rather than on experimental ones. However, there is no consensus on the actual values because theoretical and experimental estimates vary from author to author. It is thus timely to provide the theory of superconductivity a firmer experimental basis. Here we present all the dd excitation energies in several undoped layered cuprates measured by resonant inelastic x-ray scattering (RIXS) at the Cu L_3 edge.

The Cu ion in two-dimensional (2D) layered cuprates is nominally divalent (Cu^{2+}), corresponding to a 3d^9 electronic configuration. It is generally accepted that in the ground state the 3d hole on Cu is mainly found in a d$_{x^2-y^2}$ orbital [13]. dd excitations correspond to a change in the symmetry of occupied 3d states. In particular, for Cu^{2+}, the hole is excited from the d$_{x^2-y^2}$ symmetry to the d$_{3z^2-r^2}$, d$_{xy}$, d$_{xz}$ or d$_{yz}$ orbitals. dd excitations are an important ingredient for the understanding of the electronic structure of cuprates besides their possible direct implication in the mechanism of high-T_c superconductivity itself. In analogy, we can look at NiO, whose dd excitations have been studied by using optical spectroscopy [14, 15], electron energy loss spectroscopy (EELS) [16, 17] and, recently, RIXS [18]–[20]. However, although extensively investigated, *dd* excitations in cuprates are still a subject of debate because of the lack of conclusive experimental results.

Most of the experimental basis comes from optical spectroscopy. In the optical absorption of La$_2$CuO$_4$ and Sr$_2$CuO$_2$Cl$_2$, Perkins *et al* [21] found a sharp feature at 0.41 (0.36) eV, which they assigned to transitions to the d$_{3z^2-r^2}$ orbital. The same authors identified the transition to the d$_{xy}$ orbital to occur at 1.50 eV in Sr$_2$CuO$_2$Cl$_2$. Electroreflectance measurements by Falck *et al* [22] on La$_2$CuO$_4$ revealed the transitions to the d$_{xy}$ and d$_{xz/yz}$ orbitals to be at 1.40 and 1.60 eV, respectively. This scenario was compatible with crystal field calculations accompanying Cu L_3 RIXS measurements by Ghiringhelli *et al* [23] that located the transitions to the d$_{3z^2-r^2}$, d$_{xy}$ and the doubly degenerate d$_{xz/yz}$ orbitals at 0.41 (1.17), 1.38 (1.29) and 1.51 (1.69) eV for La$_2$CuO$_4$ (Sr$_2$CuO$_2$Cl$_2$). However, Lorenzana and Sawatzky [24] have previously proposed that the feature at ~ 0.4 eV in the optical absorption spectra is rather due to a phonon-assisted bimagnon excitation. More recent RIXS results by Braicovich *et al* [25] confirmed the latter assignment for La$_2$CuO$_4$ and CaCuO$_2$: the mid-infrared feature is due to magnetic excitations, dispersing up to ~ 0.40 eV, and strong dd excitations are found around 1.5–2.5 eV. This fact is also compatible with the optical Raman scattering measurements by Salomon *et al* [26], who identified the transition to the d$_{xy}$ orbital at 1.70 eV for La$_2$CuO$_4$ and 1.35 eV for Sr$_2$CuO$_2$Cl$_2$. Moreover, Cu $M_{2,3}$ edge RIXS measurements in Sr$_2$CuO$_2$Cl$_2$ by Kuiper *et al* [27] had already

located the transitions to the $d_{3z^2-r^2}$, d_{xy} and $d_{xz/yz}$ orbitals at 1.50, 1.35 and 1.70 eV, respectively (see also [23] for Cu L_3 RIXS results). Finally, direct first principle calculations by Middlemiss *et al* [28] support these findings too.

By taking advantage of the recent experimental improvements in the field of soft x-ray RIXS, we address here the problem of determining the dd excitation energies in cuprates in a systematic way. We have measured Cu L_3 RIXS spectra of La_2CuO_4 (LCO), $Sr_2CuO_2Cl_2$ (SCOC), $CaCuO_2$ (CCO) and $NdBa_2Cu_3O_6$ (NdBCO) at several sample orientations. dd excitations are shown here to have local character with no or very little dispersion versus the in-plane transferred momentum $\boldsymbol{q}_\parallel$. Using single ion theoretical cross sections we could determine the dd excitation energies for all samples with a high degree of confidence.

2. Resonant inelastic x-ray scattering

$L_{2,3}$ edge RIXS is emerging as a powerful technique for the study of neutral excitations in 3d transition metal (TM) oxides and cuprates in particular. Tanaka and Kotani [29] suggested that dd and charge transfer (CT) excitations in cuprates can be seen with this technique. It should be emphasized that, while forbidden in the optical absorption spectra by dipole selection rules, dd excitations are allowed in RIXS due to two consecutive dipole transitions. In fact, the scattering process taking place in L_3 edge RIXS can be seen as follows. Initially a $2p_{3/2}$ electron is resonantly transferred in the 3d shell through the absorption of an x-ray photon: the system is then in a highly excited state with a deep core hole. Secondly, the system decays via the transition of a 3d electron into the $2p_{3/2}$ states and the emission of a photon. As the intermediate state, characterized by a 2p core hole and an extra 3d electron, is not observed, the whole process has to be described at the second order by the Kramers–Heisenberg (KH) equation. We deal then with an energy loss spectroscopy, i.e. an inelastic scattering of x-ray photons that leaves the solid in an excited state. The energy and momentum of the final state are known from the measured variation of energy and momentum of the scattered photons. In this work we restrict ourselves to the cases where the system is left in a final configuration corresponding to a dd or spin-flip excitation.

It must be noted that local spin-flip excitations are not eigenstates of the 2D antiferromagnetically ordered lattice. Rather spin waves (magnons) are excited by Cu L_3 RIXS. Those collective excitations are known to disperse in energy as a function of their momentum and are traditionally mapped by inelastic neutron scattering (INS). In the specific case of layered cuprates, magnetic excitations are particularly difficult to measure with neutrons due to their very high energy, and only rather recently, high-quality results were obtained for La_2CuO_4 [50]. Very recently, the same type of measurements were made by Braicovich *et al* using Cu L_3 RIXS [6, 25, 31]. Thanks to the relatively large momentum carried by soft x-rays, the $\boldsymbol{q}$-dependence of single and multiple magnons could be investigated over approximately 2/3 of the first Brillouin zone (BZ). Those results were also supported theoretically [30]. It is thus clear that, thanks to the advances in instrumentation [33]–[35] that led the experimental linewidth in the 100 meV range, Cu L_3 edge RIXS has become a complementary technique to INS for the measurement of spin wave dispersion.

On the other hand, dd excitations have been studied by Cu L_3 [23] and $M_{2,3}$ edge (3p–3d) RIXS [27] with partial success. At M the lower photon energy provides a potentially better energy resolution as compared to L edge; however, because of the limited momentum carried by photons, the portion of the BZ that can be probed is limited to a region close to the Γ point. Any

possible dispersion is thus hardly detectable. Furthermore, the insufficient spin–orbit splitting of the 3p states and the extreme weakness of the inelastic cross section with respect to the elastic scattering make the analysis and interpretation of the experimental data very difficult. It is interesting to note that dd excitations have also been seen at Cu K edge RIXS [36] but in this case dd are much weaker than CT excitations because they are indirectly excited.

3. Experimental information

LCO, SCOC and NdBCO measurements were carried out at the ADRESS beamline [32] of the Swiss Light Source at the Paul Scherrer Institute (SLS-PSI) in Villigen (CH) using the SAXES [33] spectrometer. At the Cu L_3 edge (approximately 930 eV) the combined energy resolution is $\Delta E = 130$ meV full-width at half-maximum (FWHM) with a data point sampling of 14.1 meV data point^{-1}. CCO RIXS spectra were recorded at the ID08 beamline of the European Synchrotron Radiation Facility (ESRF) in Grenoble (FR) using the AXES [34, 35] spectrometer. The combined energy resolution here was $\Delta E = 240$ meV FWHM (31.0 meV data point^{-1}) at the same incident energy. In both cases, the incident photon energy was finely tuned at the L_3 peak by inspection of the absorption spectrum. The linear polarization of the incident beam could be set either perpendicular (vertical polarization, σ, hereafter) or parallel (horizontal, π) to the scattering plane. The polarization of the outgoing beam was not detected. Spectra were obtained as the sum of 6–12 partial spectra of 5 or 10 min each. Off resonance elastic peaks were periodically measured on a graphite powder to determine the zero energy loss of the spectra. The pressure in the measurement vacuum chamber was better than 3×10^{-9} mbar. All the measurements were carried out at 15 K (except LCO that was measured at room temperature).

In figure 1, the scattering geometry is shown. The beam hits the sample surface at incident angles θ_i and ϕ_i and the outgoing beam is collected at angles θ_o and ϕ_o in the xyz reference system; in general the scattering angle 2θ is determined by θ_i, ϕ_i, θ_o and ϕ_o, but in our case $\phi_o = \phi_i$ so that 2θ depends only on θ_i and θ_o. The momentum $\boldsymbol{q}$ transferred to the sample due to the scattering process is shown by the red arrow. Its projection onto the sample ab-plane ($\boldsymbol{q}_\parallel$) is also shown because the meaningful reciprocal space is usually 2D. The scattering angle 2θ is fixed at 130° for the AXES spectrometer, whereas it could be set at either 90° or 130° for SAXES, in all cases lying in the horizontal plane. It should be noted that, for a fixed 2θ, $\boldsymbol{q}$ is fixed, but $\boldsymbol{q}_\parallel$ can be easily changed in both magnitude and direction in the sample 2D reciprocal space by rotating the sample itself around an axis perpendicular or parallel to the scattering plane. For the sake of simplicity, we introduce the angle δ between the transferred momentum $\boldsymbol{q}$ and the sample c-axis, lying in the scattering plane. With this notation, $|\boldsymbol{q}_\parallel| = 2|\boldsymbol{k}| \sin(\theta) \sin(\delta)$, where $\boldsymbol{k} = \boldsymbol{k}_i \; (\approx \boldsymbol{k}_o)$ is the momentum carried by ingoing (outgoing) photons. For example, when $\delta = 0$ (specular geometry), $\boldsymbol{q}$ is parallel to the sample c-axis and $\boldsymbol{q}_\parallel = 0$, thus allowing us to probe excitations in the center of the BZ. On the other hand, if one could go to infinitely grazing incidence (emission), then $\delta = -\theta \; (+\theta)$ and the maximum magnitude of $\boldsymbol{q}_\parallel$ would then be reached. The value of $\boldsymbol{q}$ depends on the scattering angle: at $\hbar\omega_i = 930$ eV, $\boldsymbol{q}_{\parallel max}$ is equal to 0.47 Å^{-1} for $2\theta = 90°$, and 0.77 Å^{-1} for $2\theta = 130°$. All the measurements were carried out at a fixed scattering angle 2θ and by changing δ by rotating the sample around an axis vertical in the laboratory space and perpendicular to the scattering plane, in steps of 5° typically. Samples were aligned so to have $\boldsymbol{q}_\parallel$ parallel to the [10] direction ($\phi_i = 0$) or the [11] direction ($\phi_i = 45°$) in the BZ.
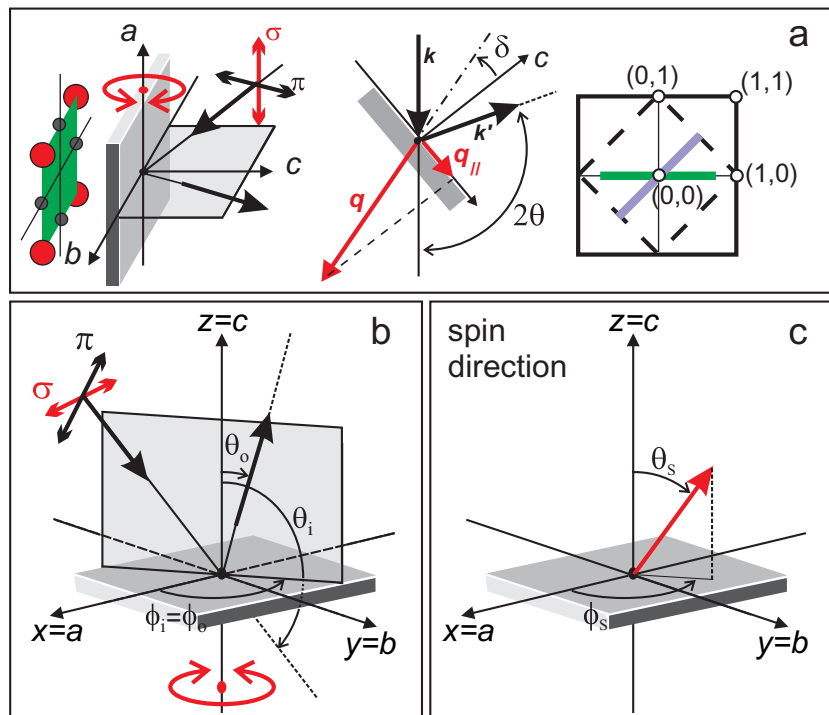
Figure 1. (a, b) The experimental geometry is shown. The incoming beam hits the sample surface (assumed to be parallel to the ab plane) at incident angles θ_i and ϕ_i and the outgoing beam is collected at the angles θ_o and ϕ_o. The scattering angle 2θ is fixed, whereas the incident angle and the azimuthal angle can be changed. They define δ, the angle between the sample c-axis and the transferred momentum q (red arrow). The projection of q onto the sample ab-plane, $q_\parallel$, is also shown. In the experiment δ is changed by rotating the sample around a vertical axis. In this way, the regions of the 2D reciprocal space indicated by thick lines can be covered (panel (a), to the right). The [1, 0] and [1, 1] directions correspond to $\phi_i = 0$ and $45°$, respectively. (c) The orientation of the atomic spin moments is also a parameter in the cross-section calculations.

100 nm thick LCO and CCO films were grown by pulsed laser deposition on (001) $SrTiO_3$ single crystals. An excimer laser charged with KrF ($\lambda = 248$ nm, 25 ns pulse width) was used at a laser fluence of about $2\,J\,cm^{-2}$ at the target. Growth temperatures were $800\,°C$ for LCO and $650\,°C$ for CCO. A partial oxygen pressure of about 0.1 mbar was employed to correctly oxidize the films during deposition. In the case of LCO the quality of the films was also *in situ* controlled by the reflection high-energy electron diffraction (RHEED) technique. The SCOC sample was laminar-like single crystals obtained by the slow cooling in air of a melt of $Sr_2CuO_2Cl_2$ powder. X-ray powder diffraction (XRD) analysis was conducted on a Rigaku x-ray diffractometer with Cu Kα radiation ($\lambda = 1.5418\,Å$) and the electron microprobe was used for chemical analysis. 100 nm thick $Nd_{1.2}Ba_{1.8}CuO_{6+x}$ ($x < 0.1$) film were deposited on $SrTiO_3$ (100) single crystals by diode high-pressure oxygen sputtering. Undoped NdBCO thin films were obtained by reducing the oxygen content by annealing as-grown $Nd_{1.2}Ba_{1.8}CuO_{7-\delta}$ samples in argon atmosphere (10 mbar) for 24 h. The structural and morphological properties
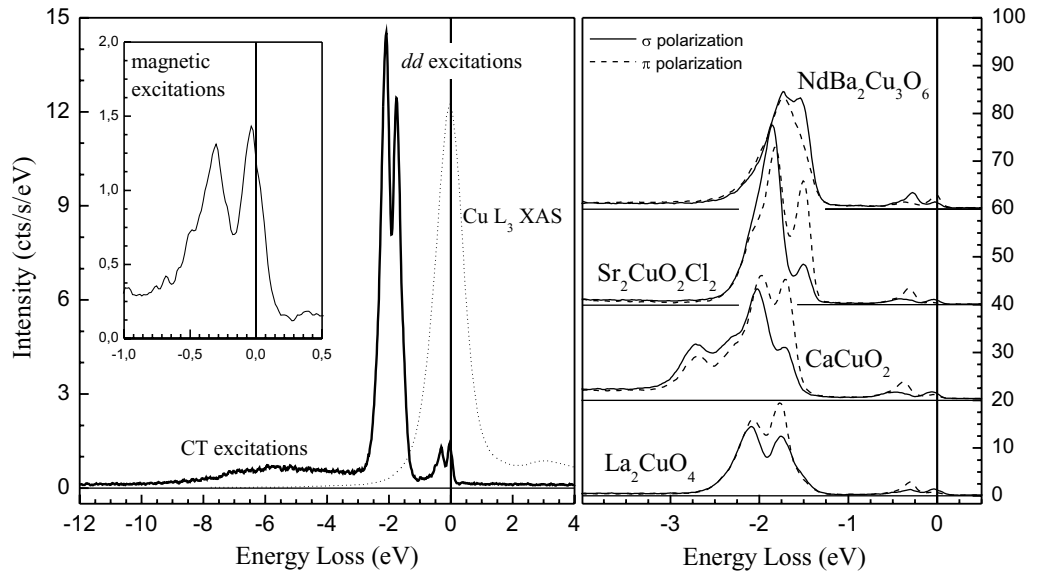
Figure 2. (Left panel) Example of Cu L_3 absorption (dashed) and RIXS (solid) spectra of LCO with σ polarization. For RIXS the angles were set to $2\theta = 130°$, $\delta = +45°$ (i.e. $20°$ grazing emission) and $\phi_i = 0$. One can immediately recognize at CT, dd and magnetic excitations at different energy ranges. A closer look at the mid-infrared energy region is given in the inset. (Right panel) RIXS spectra for LCO, SCOC, CCO and NdBCO in the same experimental geometry as the left panel.

of the sample have been checked by x-ray diffraction, using synchrotron radiation and by atomic force microscopy [38]. The samples are tetragonal and perfectly matched with the STO lattice ($a = b = 3.905$ Å) while the c-axis is 11.81 Å.

For LCO, CCO, NdBCO and SCOC, the fraction of the BZ that could be explored along the [10] direction was 93.1, 94.4, 95.6 and 97.3%, respectively, for $2\theta = 130°$. In the case of LCO and SCOC, it decreased to 56.9 (59.4)% with 2θ set at $90°$. Moreover, in the case of SCOC, measurements along the [11] direction were taken up to 68.8% of the nuclear BZ boundary with $2\theta = 130°$, i.e. the whole magnetic BZ could be spanned.

4. Experimental spectra and cross-section calculations

4.1. Overview of experimental spectra

In the left panel of figure 2(a), the Cu L_3 edge RIXS spectrum with σ polarization of LCO is shown. The scattering angle 2θ was set at $130°$ and the sample was rotated at $\delta = +45°$, i.e. $20°$ grazing emission, and $\phi_i = 0$ ($q_\parallel$ parallel to the [10]-direction in reciprocal space). The very high resolution allows us to clearly recognize different excitations depending on the energy scale. The spectrum is dominated by dd excitations, which will be extensively discussed below. Both at higher and lower energies other features are found with a much (approximately one order of magnitude) lower counting rate. Excitations in the mid-infrared region (up to ~ 500 meV) are expanded in the inset and are known to have a magnetic character: they are a combination of

a dispersing magnon, a continuum given by bimagnons and other multi-magnon excitations, phonon peaks and an elastic zero-loss line [6, 25, 31]. At higher energies CT excitations are also visible, as a broad distribution, via the Cu 3d–O 2p hybridization. By looking at the absorption spectrum (dashed line), it can also be noted that features above 1 eV energy loss, such as dd excitations, are weakly affected by self-absorption because of the reduced absorption coefficient 2 eV below the resonance peak. In the right panel of figure 2, dd excitations of LCO are compared to those of SCOC, CCO and NdBCO for both σ (solid) and π (dashed line) polarizations. The effect of changing the incident photon polarization is considerable. The spectral shape changes drastically for the four compounds, reflecting differences in the Cu^{2+} coordination. In order to recognize the symmetry of the RIXS final state, we carried out systematic measurements with both polarizations as a function of δ (or θ_i, accordingly) for a fixed 2θ and fitted the spectra to obtain an estimate of the dd excitation energies. The fitting procedure is presented in the following subsection and is based on single-ion model calculations of the RIXS cross sections.

4.2. Single-ion model cross section calculations

In cuprates, Cu ions are known to be mostly in the Cu^{2+} oxidation state [42] corresponding to a $3d^9$ electronic configuration. In the crudest approximation, we only consider the atomic states of a Cu^{2+} ion. RIXS is a second-order process and is described by the KH equation. The scattering is here modeled in two steps: first one $2p_{3/2}$ electron is resonantly promoted into the 3d states by absorption of a photon (intermediate state). Because of the large 2p spin–orbit splitting (~ 20 eV), interference effects with the $2p_{1/2}$ states can be neglected. The only available intermediate state is given by a fully occupied 3d shell and one hole in the fourfold degenerate $2p_{3/2}$ core level. The second step is the radiative deexcitation of one 3d electron into the $2p_{3/2}$ levels. In short notation, the process can be written as the sequence $2p_{3/2}^4 3d^9 \rightarrow 2p_{3/2}^3 3d^{10} \rightarrow 2p_{3/2}^4 3d^{9*}$, where the $*$ indicates that the final states can be either the ground state or an excited state with the 3d hole occupying a state with different orbital symmetry and/or spin.

Matrix elements entering the KH equation for the calculation of the RIXS cross sections are here calculated in the atomic approximation as follows. We consider the scattering ion as a hydrogen-like system of a single positively charged particle (hole) and we express the angular part of the one-particle wave functions (p and d orbitals) in spherical harmonics. The radial part of the integrals is the same for all the considered transitions and is thus neglected also in the expressions of the 2p and 3d states. The local symmetry is D_{4h}, so the commonly used set of atomic d orbitals is well suited to represent the atomic states in terms of symmetry:

$$d_{x^2-y^2} = \frac{1}{\sqrt{2}}(Y_{22} + Y_{2\bar{2}}), \tag{1}$$

$$d_{3z^2-r^2} = Y_{20}, \tag{2}$$

$$d_{xy} = -\frac{i}{\sqrt{2}}(Y_{22} - Y_{2\bar{2}}), \tag{3}$$

$$d_{yz} = -\frac{i}{\sqrt{2}}(Y_{21} + Y_{2\bar{1}}), \tag{4}$$

$$d_{xz} = \frac{1}{\sqrt{2}} (Y_{21} - Y_{2\bar{1}}) . \tag{5}$$

The latter two are degenerate for D_{4h} symmetry. As, in all layered cuprates, the four in-plane O ions are the Cu nearest neighbors, the unique 3d hole present in the ground state has an almost pure $x^2 - y^2$ character [13]. Thus the dd excitations can be described as the transfer of the 3d hole from the $d_{x^2-y^2}$ orbital to the $d_{3z^2-r^2}$, d_{xy}, d_{yz} or d_{xz} orbitals. Also the case of $d_{x^2-y^2}$ final state can be viewed as a dd excitation, giving rise to an elastic scattering or to a pure spin-flip excitation depending on the final spin state.

Superimposed on the CF splitting of 3d orbitals is the additional spin splitting of each state due to super-exchange interaction with neighboring in-plane Cu^{2+} ions (spin–orbit of 3d states is neglected), which doubles the number of possible final states. In this work, we will not consider the low energy part of the spectra because the description of the set of possible final states cannot be done in a single-ion model. In fact, the local spin-flip is not an eigenstate of the 2D Heisenberg AFM lattice: spin waves should then be introduced to account for the dispersion of pure magnetic excitations, as already demonstrated in [6, 30].

Although we do not look at pure magnetic excitations, in order to correctly calculate the RIXS cross sections the local atomic spin orientation has to be explicitly taken into account. As the 3d spin–orbit interaction is weak in Cu [37], spin is a good quantum number for both the ground and final states. We use here the Pauli matrices $\tilde{\sigma}_x$, $\tilde{\sigma}_y$ and $\tilde{\sigma}_z$. The arbitrary spin orientation of the initial hole is defined by the angles θ_s and ϕ_s and the eigenvectors of

$$\tilde{\sigma}(\theta_s, \phi_s) = (\tilde{\sigma}_x \cos \phi_s + \tilde{\sigma}_y \sin \phi_s) \sin \theta_s + \tilde{\sigma}_z \cos \theta_s \tag{6}$$

give the weights for spin-up and spin-down components along z for the generic spin direction. For instance, if we assume the ground state spin direction to be 'down' in the hole representation, the ground state wave function and the spin-flip wave function are written as

$$d_{x^2-y^2}^{\downarrow} = \frac{1}{\sqrt{2}} \left[U_-(Y_{22}^{\uparrow} + Y_{2\bar{2}}^{\uparrow}) + D_-(Y_{22}^{\downarrow} + Y_{2\bar{2}}^{\downarrow}) \right], \tag{7}$$

$$d_{x^2-y^2}^{\uparrow} = \frac{1}{\sqrt{2}} \left[U_+(Y_{22}^{\uparrow} + Y_{2\bar{2}}^{\uparrow}) + D_+(Y_{22}^{\downarrow} + Y_{2\bar{2}}^{\downarrow}) \right], \tag{8}$$

where U_- (U_+) and D_- (D_+) are the components of the eigenvector corresponding to the negative (positive) eigenvalue of $\tilde{\sigma}(\theta_s, \phi_s)$. The same holds for the other 3d orbitals that, together with the ground state itself and the spin-flip state, represent the ten different possible final states available for the transition, i.e $d_{x^2-y^2}^{\downarrow}$, $d_{x^2-y^2}^{\uparrow}$, $d_{3z^2-r^2}^{\downarrow}$, $d_{3z^2-r^2}^{\uparrow}$, $d_{xy}^{\downarrow}$, $d_{xy}^{\uparrow}$, $d_{xz}^{\downarrow}$, $d_{xz}^{\uparrow}$, $d_{yz}^{\downarrow}$ and $d_{yz}^{\uparrow}$.

In contrast 2p states are strongly spin–orbit coupled and spin is not a good quantum number; the energetically degenerate $2p_{3/2}$ orbitals are written in terms of spherical harmonics as follows:

$$p_{3/2,-3/2} = Y_{1\bar{1}}^{\downarrow}, \tag{9}$$

$$p_{3/2,-1/2} = \sqrt{\frac{1}{3}} Y_{1\bar{1}}^{\uparrow} + \sqrt{\frac{2}{3}} Y_{10}^{\downarrow}, \tag{10}$$

$$p_{3/2,1/2} = \sqrt{\frac{2}{3}} Y_{10}^{\uparrow} + \sqrt{\frac{1}{3}} Y_{11}^{\downarrow}, \tag{11}$$

$$p_{3/2,3/2} = Y_{11}^{\uparrow}. \tag{12}$$

In the approximation that the lifetimes of the $2p_{3/2}$ states are the same, the RIXS transition from the ground state $d^{\downarrow}_{x^2-y^2}$ to a given final state, say $d^{\downarrow(\uparrow)}_{3z^2-r^2}$, is given by

$$\sigma^{\downarrow(\uparrow)}_{3z^2-r^2} \propto \sum_{q'} \left| \sum_m \langle d^{\downarrow(\uparrow)}_{3z^2-r^2} | T^{\dagger}_{q'} | p_{3/2,m} \rangle \langle p_{3/2,m} | T_q | d^{\downarrow}_{x^2-y^2} \rangle \right|^2, \tag{13}$$

where $m = -\frac{3}{2}, -\frac{1}{2}, \frac{1}{2}, \frac{3}{2}$ runs over the intermediate states. $T_q = \sqrt{4\pi/(2q+1)} Y_{1q}(\theta, \phi)$ is the expression for the electric dipole operator in spherical harmonics with $q = -1, 0, 1$ for *left*, *linear* (z) and *right* polarized light, respectively. The sum over q' is required because we do not measure the polarization of the outgoing photons in our experiments. Matrix elements are thus simple integrals of three spherical harmonics which can be readily calculated [43].

Using this method we can calculate the scattering cross section for all the dd excitations of cuprates for any incident and scattered directions and polarization of the photons and any atomic spin direction. For example, if the atomic spin is oriented along the [110] direction ($\theta_s = 90°$ and $\phi_s = 45°$) and $2\theta = 90°$, the cross sections for the elastic and pure spin-flip transitions are given by the simple formulae

$$\sigma^{\downarrow}_{x^2-y^2,\sigma} \propto 4, \tag{14}$$

$$\sigma^{\uparrow}_{x^2-y^2,\sigma} \propto \sin^2 \theta_i \tag{15}$$

in the case of incident σ polarization and

$$\sigma^{\downarrow}_{x^2-y^2,\pi} \propto \sin^2 2\theta_i, \tag{16}$$

$$\sigma^{\uparrow}_{x^2-y^2,\pi} \propto \cos^2 \theta_i \tag{17}$$

in the case of incident π-polarization and the scattering plane perpendicular to the sample surface.

In figure 3, the calculated cross sections are shown in the two particular cases $\phi_i = 0$ and $\phi_i = 45°$ as a function of θ_i or alternatively of the in-plane transferred momentum $q_{\parallel}$ for $2\theta = 90°$ (left panel) and $2\theta = 130°$ (right panel). We highlight that, contrary to what was previously stated in the literature [43, 44], pure spin-flip transitions are allowed as long as the spin is not parallel to the [001] direction [30] (see the curves labeled $\sigma \uparrow$ and $\pi \uparrow$ for the $x^2 - y^2$ final state in figure 3). For layered cuprates, this selection rule has the important consequence that single magnons can contribute to the Cu L_3 edge RIXS spectrum [30] since here spins are known to lie always in the *ab*-plane [39, 45, 46]. We highlight the fact that the orientation of the spin within the *ab*-plane has no influence on the spin-flip cross section. This makes it simpler to measure the magnon dispersion in samples with multiple magnetic domains. However, some of the dd cross sections do depend on the ϕ_s value (having fixed $\theta_s = 90°$). By this dependence one could think of using the dd excitation spectrum to determine the in-plane orientation of the spin in layered cuprates.

Calculations are then used to determine the energy and symmetry of Cu-3d states by fitting the experimental data. It is important to note that cross sections are here calculated on the basis of symmetry properties of the angular part of the ground state and final state wave functions.

IOP Institute of Physics **Φ** DEUTSCHE PHYSIKALISCHE GESELLSCHAFT
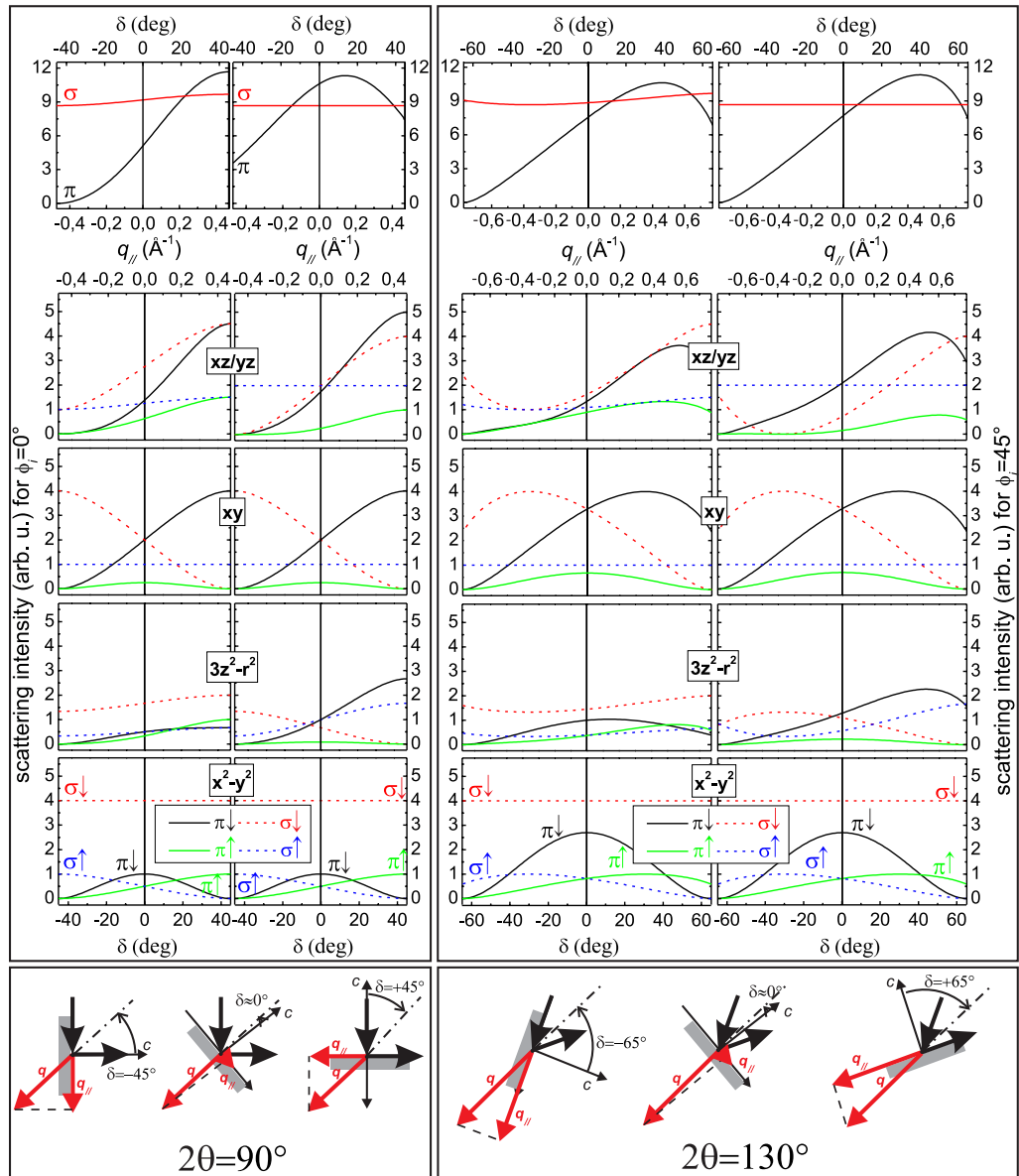
Figure 3. Single-ion Cu^{2+} L_3 edge RIXS cross section for $2\theta = 90°$ (left panel) and $2\theta = 130°$ (right panel) and for two different angles $\phi_i = 0$ and $\phi_i = 45°$ for both σ and π polarizations. The bottom panels show sketches of the experimental geometry. The spin is fixed in the calculation along the [110] direction ($\theta_s = 90°$, $\phi_s = 45°$). All the possible dd excitations including the elastic and spin-flip final states are considered. As already explained in figure 1, to a given δ (bottom axis scale) corresponds an in-plane transferred momentum $q_\parallel$ (top axis scale). In the top panels, the sums of all dd excitations (excluding elastic and spin-flip) cross sections are given.

By including the Cu 3d–O 2p hybridization the symmetry of the problem would not change [47, 48] and the dependence on the scattering geometry and photon polarization would remain the one calculated here, as it depends solely on symmetry properties [48].

Once the cross sections for all the possible final states are calculated, one has to construct the simulated spectra as a function of the energy loss ($\hbar\omega_o - \hbar\omega_i$) as

$$I(\hbar\omega_o - \hbar\omega_i) = \frac{1}{\pi} \sum_f \left[\frac{\Gamma_f \sigma_f^{\downarrow}}{\left(\hbar\omega_o - \hbar\omega_i + E_f\right)^2 + \Gamma_f^2} + \frac{\Gamma_f \sigma_f^{\uparrow}}{\left(\hbar\omega_o - \hbar\omega_i + E_f + 2J_f\right)^2 + \Gamma_f^2} \right], \quad (18)$$

where f runs over $x^2 - y^2$, $3z^2 - r^2$, xy, xz and yz. We assume here that the Lorentzian lifetime broadening Γ_f is equal for states with the same orbital symmetry, while the super-exchange coupling (J_f) is orbital dependent. From overlap considerations [49], one finds that $J_{3z^2-r^2} = J_{x^2-y^2}/6 = J/6$ and $J_{xy} = J_{xz} = J_{yz} = 0$. J_f gives the energy separation between a peak and its spin-split satellite: according to the 2D Ising model, in the ground state the energetic cost to flip one spin is $2J$, while in the excited states the exchange constant is reduced because of the smaller overlap with nearest neighbor orbitals. In this work, we have fixed $J = 130$ meV for all samples for simplicity, although it is known that its value is different ($\pm 20\%$) from sample to sample. Indeed this difference would have little effect on our calculated spectra, due to the strong reduction or cancelation of J_f with respect to J as explained above.

Finally, E_f is the energy of the final state with a given symmetry (f) and spin down ($\downarrow$). Geometry and polarization dependences that enter the simulations through σ_f are obviously fixed by the experiment. This imposes a severe constraint on the number of free fitting parameters, which is thus limited to the energy positions of the 3d states (namely $E_{3z^2-r^2}$, E_{xy} and $E_{xz/yz}$, while $E_{x^2-y^2} = 0$ by definition) and to their Lorentzian lifetime broadening ($\Gamma_{3z^2-r^2}$, Γ_{xy} and $\Gamma_{xz/yz}$). The energies (E_f) of the final states should be considered as effective energies, thus taking into account both the ionic and the covalent part of the bond. Figure 4 shows an example of the fitting procedure for LCO ($\delta = 0$, $2\theta = 90°$, σ polarization). Thick blue lines are δ-like functions whose heights are proportional to the calculated cross sections (σ_f); they are convoluted with Lorentzian functions to take into account the lifetime broadening of the final states (Γ_f) to obtain the dashed curves. Their sum gives the red dashed line, which is eventually convoluted with a Gaussian (whose FWHM matches the effective experimental resolution) to obtain the simulated Cu L_3 edge RIXS spectrum (red line).

5. Determination of dd excitation energies and discussion

5.1. Fitting results

In this section, the experimental trends are shown together with the results of the simulations. In figure 5, measured and calculated RIXS spectra of LCO are compared, for both $2\theta = 90°$ and $2\theta = 130°$ with $\phi_i = 0$. From the top spectrum to the bottom one, δ is changed in steps of $5°$ from $10°$ grazing emission to $10°$ grazing incidence. As the incidence angle is changed, $q_{\parallel}$ varies accordingly. However, it is evident from the experimental results that the dispersion of dd excitations, if any, is very small for both $2\theta = 90°$ and $2\theta = 130°$. This finding seems to be general and holds true also in the cases of SCOC (figures 6 and 7), CCO (figure 8) and NdBCO (figure 9). Within the present experimental accuracy, the dd excitations do not disperse in any of the undoped layered cuprates measured by us.

The fact that dd excitations are fixed in energy when changing δ allowed us to fit all the spectra for a given sample using fixed values of E_f and Γ_f. Using the redundancy of the experimental basis the values of the free parameters E_f and Γ_f could thus be optimized. The high degree of confidence reached is made evident by the excellent agreement of the fitted
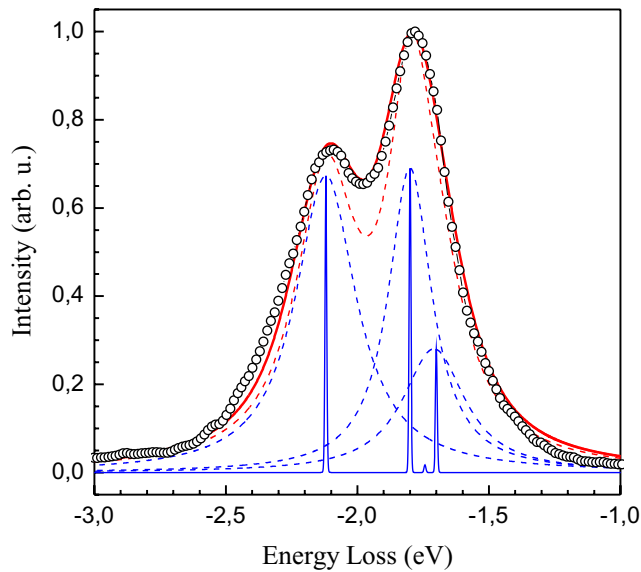
Figure 4. Cu L_3 edge RIXS spectrum (open circles) of LCO taken at $\delta = 0$, $2\theta = 90°$ and σ polarization. The theoretical spectrum is built by convoluting delta functions proportional to the calculated cross sections σ_f (thick blue) with Lorentzians to include finite lifetime broadening (dashed blue). Their sum gives the hypothetical spectrum measured with infinite resolution (dashed red). The spectrum to be compared to the experimental results is obtained after convolution with a Gaussian curve (solid red). The energy of various dd excitations (E_f) and the Lorentzian widths (Γ_f) are used as adjustable parameters in the fitting procedure.

spectra to the experimental ones shown in the figures. For clarity we recall here the input parameters of our fitting. The RIXS cross sections σ_f are calculated for each final state within the ionic model; the superexchange interaction is fixed to $J = 130$ meV for all samples; the Gaussian broadening is set to 130 meV FWHM; the energy E_f and Lorentzian broadening Γ_f are the free parameters for optimizing the fitting and are thus the result of the comparison of calculated and measured spectra.

The results for the four samples are summarized in table 1. For LCO and SCOC, we used the data measured at both $2\theta = 90°$ and $130°$ for $\phi_i = 0$. For SCOC we employed data with $2\theta = 130°$ and $\phi_i = 45°$. For CCO and NdBCO the data used were at $2\theta = 130°$ and $\phi_i = 0$ only. Although the spectra of CCO shown in figure 8 were measured with lower resolving power ($\Delta E = 240$ meV), the fitting results are perfectly compatible with the (few) spectra taken at higher resolution ($\Delta E = 130$ meV) of figure 2. However, here the better resolution makes evident an additional feature at about 2.4 eV, which could not be assigned within our model. Possibly the extra peak could be related to oxygen vacancies affecting the local environment of Cu ions. Independent results on magnetic excitations of the same sample [52] seem to further support this interpretation.

Finally, we note that the fitting works well for NdBCO too, in spite of the presence in this sample of two different Cu sites. Namely, in this YBCO-like system, Cu ions can be
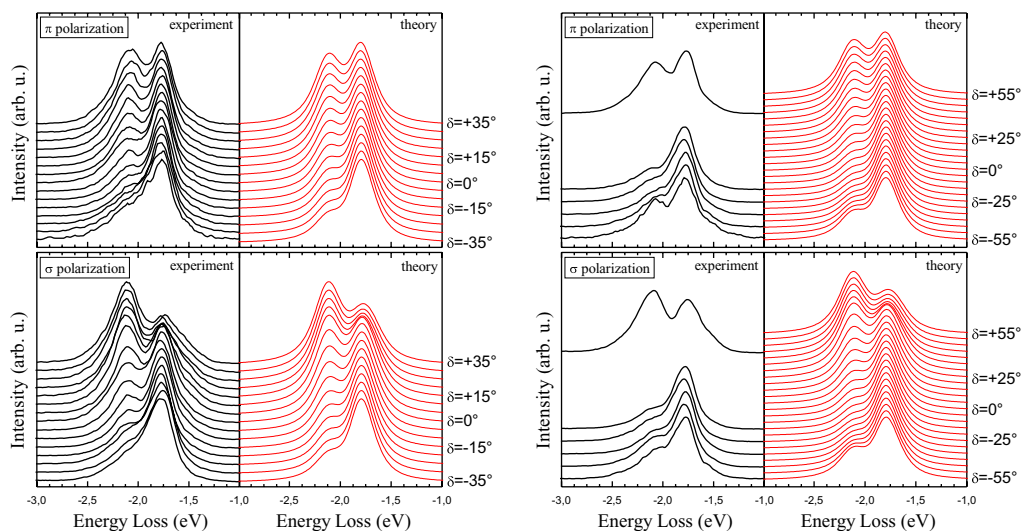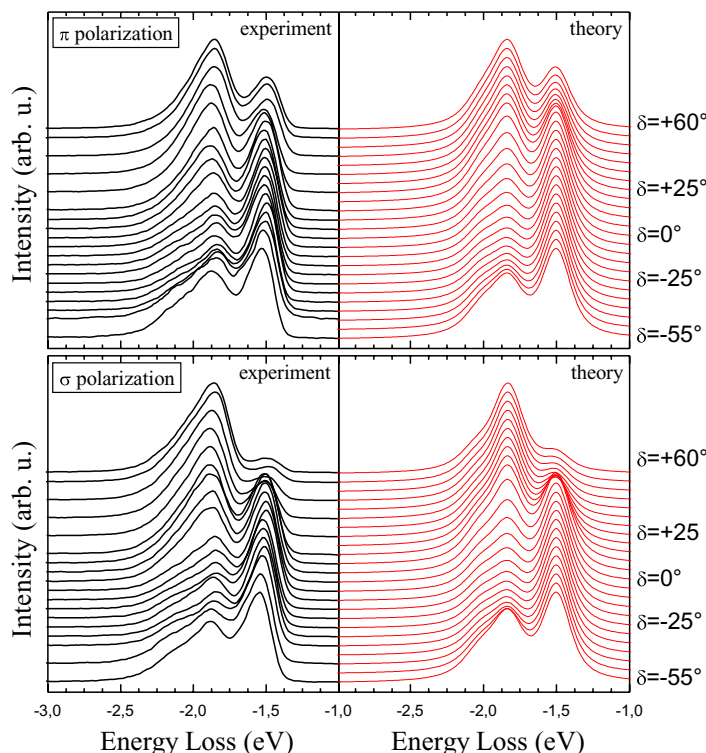
Figure 5. Measured (black line) and calculated (red line) RIXS spectra of LCO for various δ, ranging from $10°$ grazing incidence to $10°$ grazing emission with respect to the sample surface in steps of $5°$. Dispersion along the [10] direction: $\phi_i = 0$; $2\theta = 90°$ (left panel) and $2\theta = 130°$ (right panel).
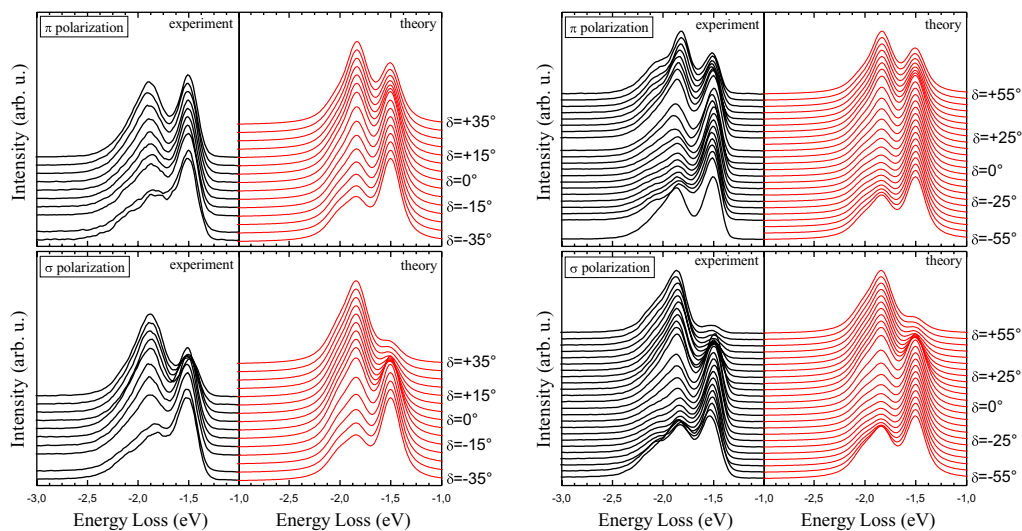
Figure 6. Measured (black line) and calculated (red line) RIXS spectra of SCOC for various δ, ranging from $10°$ grazing incidence to $10°$ grazing emission with respect to the sample surface in steps of $5°$. Dispersion along the [10] direction: $\phi_i = 0$; $2\theta = 90°$ (left panel) and $2\theta = 130°$ (right panel).

found also outside the CuO_2 planes, in the so-called CuO chains (although in this undoped compound chains are actually broken). As, in the simulations, we assume that only one species is contributing to the RIXS spectrum, we attribute this result to the extreme selectivity provided by the resonance in the excitation step.
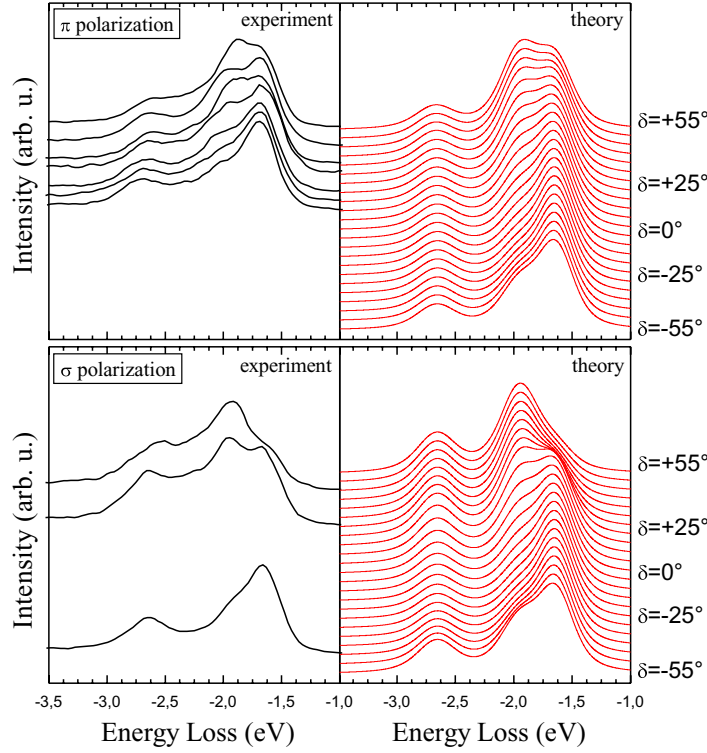
Figure 7. Measured (black line) and calculated (red line) RIXS spectra of SCOC for various δ, ranging from $10°$ grazing incidence to $10°$ grazing emission with respect to the sample surface in steps of $5°$. Dispersion along the [11] direction: $\phi_i = 45°$; $2\theta = 130°$.

5.2. *Discussion*

The energies of the 3d states obtained through our RIXS measurements are evidently related to the local coordination of Cu ions (symmetry and atomic distances). In fact, the four materials share the fourfold planar coordination that gives the famous CuO_4 plaquettes present in all cuprate superconductors. However, the in-plane Cu–O distances vary from a minimum in LCO to a maximum in SCOC: the lattice parameters are $a = 3.80$ Å for LCO [39], 3.85 Å for CCO [40], 3.90 Å for NdBCO [41] and 3.97 Å for SCOC [39]. The out-of-plane coordination is even more diverse. CCO has no apical ligands and, because of that, it is often called an infinite layer compound. Both LCO and SCOC have two apical ligands, symmetric with respect to the basal plane, at larger distance than the in-plane O (tetragonally distorted octahedral symmetry); in LCO, apical O^{2-} ions are 2.43 Å from Cu^{2+}; in SCOC, Cl^- ions are at 2.86 Å. Finally, NdBCO has a double layer YBCO-like structure, i.e. only one apical oxygen 2.27 Å from the CuO_2 plane.

The relation of the dd excitation energies to the local structural properties of our samples is evident and relatively simple. Before comparing the results to any theoretical model, we highlight these relations in a purely phenomenological way. The experimentally determined energies for each final state symmetry are listed in table 1 and refer to the x^2-y^2 ground state. A graphical presentation is given in figure 10. We also used the results of $Sr_{0.5}Ca_{0.5}CuO_2$ (SCCO, the same structure as CCO but with larger in-plane lattice parameter $a = 3.90$ Å),
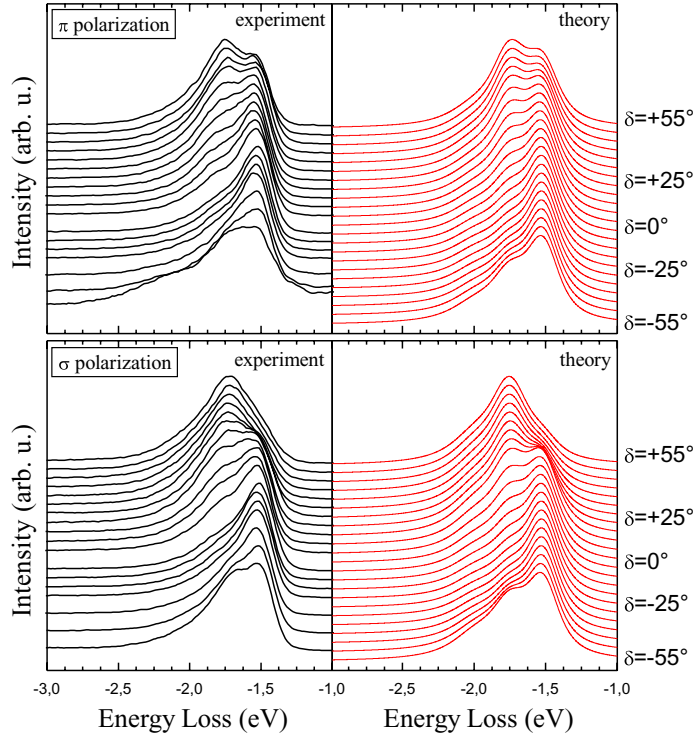
Figure 8. Measured (black line) and calculated (red line) RIXS spectra of CCO for various δ, ranging from $10°$ grazing incidence to $10°$ grazing emission with respect to the sample surface in steps of $5°$. Dispersion along the [10] direction: $\phi_i = 0$; $2\theta = 130°$.

although the spectra are not shown here [52]. The xy excitation energy increases with decreasing a. When displayed on a logarithmic scale a power relation can be highlighted: a best fit to our data gives $E_{xy} \propto a^{-4.2}$. The splitting of the t_{2g} states ($\Delta_{t_{2g}} = E_{xz/yz} - E_{xy}$) is rather small and almost independent of the out-of-plane lattice parameter l and of the presence of apical ligands. In contrast, the splitting of the e_g states ($\Delta_{e_g} = E_{3z^2-r^2} - E_{x^2-y^2}$) varies considerably from sample to sample but a univocal trend versus the Cu–ligand distances ($a/2$ and l) cannot be found due to the other parameters at play (ligand element and valence, symmetry with respect to the basal plane). However, if we do not consider NdBCO, which has a pyramidal coordination, a qualitative trend emerges: the e_g splitting increases when the apical ligand is farther from the Cu ion. And the energy of the $3z^2 - r^2$ state differs as much as almost 1 eV in LCO and CCO. This demonstrates that the local coordination can hugely impact the e_g splitting.

The widely known CF model can be used to understand the trends in the experimental results. We take a single-site, purely ionic picture, where the energies of the 3d orbitals are determined by the symmetry and strength of the non-central Coulomb field produced by the charged ligands near the central Cu^{2+} ion. Besides an addictive constant, the energy levels of d states in the tetragonally distorted octahedral symmetry are usually written as [53]

$$E_{x^2-y^2}^{CF} = 6Dq + 2D_s - D_t, \tag{19}$$

$$E_{3z^2-r^2}^{CF} = 6Dq - 2D_s - 6D_t, \tag{20}$$

Figure 9. Measured (black line) and calculated (red line) RIXS spectra of NdBCO for various δ, ranging from $10°$ grazing incidence to $10°$ grazing emission with respect to the sample surface in steps of $5°$. Dispersion along the [10] direction: $\phi_i = 0$; $2\theta = 130°$.
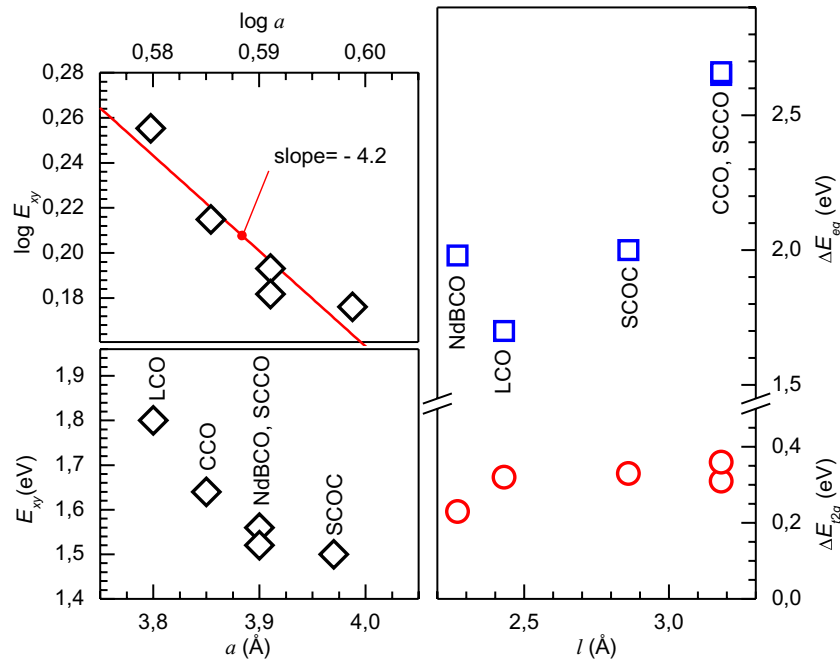
$$E_{xy}^{\text{CF}} = -4Dq + 2D_s - D_t, \tag{21}$$

$$E_{xz/yz}^{\text{CF}} = -4Dq - D_s + 4D_t, \tag{22}$$

where Dq (or $10Dq$), D_s and D_t are the CF parameters depending on the geometrical arrangement of point charges around the Cu^{2+} ion. In particular, $10Dq$ gives the energy splitting between the e_g and t_{2g} orbitals, while $4D_s + 5D_t$ and $3D_s - 5D_t$ give the splitting of e_g (ΔE_{e_g}) and t_{2g} ($\Delta E_{t_{2g}}$) orbitals, respectively (see figure 11). It can be shown [53] that within the CF model $10Dq$ scales with a power law of the in-plane lattice parameter a, i.e. $10Dq \sim a^{-n}$, with $n = 5$. The value of the effective CF parameters $10Dq$, D_s and D_t were determined by comparison with the experimental results and are given in table 1. The single-ion CF model neglects completely the Cu–ligand orbital overlaps and some important physical properties are totally missing, such as the super-exchange interaction. However, it can capture the power law dependence of E_{xy} on a, although the exponent n is overestimated ($n = 5$ instead of 4.2). On the other hand, although it is always possible to find a combination of $10Dq$, D_s and D_t compatible with the experimental results, it might happen that their values have little physical meaning. In particular, $10Dq$, which is widely used in various calculations from single-ion to cluster or impurity models, has to be regarded here as an *effective* parameter, i.e. the value obtained in CF cannot be applied directly to other models.

On the other hand, one can tentatively try to include the effect of covalency with the help of 2D-cluster calculations: Eskes *et al* [47] proposed a cluster-model calculation of the electronic

Table 1. Parameters used in the calculations to fit the experimental data. Also listed are the values of the effective CF parameters and those for a pure covalent picture within a 2D cluster. In all cases except the LCO case, covalent parameters could not be defined (n.d.) as explained in the text. For all samples the superexchange J was fixed at 130 meV.

	La_2CuO_4	$Sr_2CuO_2Cl_2$	$CaCuO_2$	$Sr_{0.5}Ca_{0.5}CuO_2$	$NdBa_2Cu_3O_7$
$E_{3z^2-r^2}$ ($\Gamma_{3z^2-r^2}$) (eV)	1.70 (0.14)	1.97 (0.10)	2.65 (0.12)	2.66	1.98 (0.18)
E_{xy} (Γ_{xy}) (eV)	1.80 (0.10)	1.50 (0.08)	1.64 (0.09)	1.56	1.52 (0.10)
$E_{xz/yz}$ ($\Gamma_{xz/yz}$) (eV)	2.12 (0.14)	1.84 (0.10)	1.95 (0.12)	1.93	1.75 (0.12)
ΔE_{e_g}	1.70	1.97	2.65	2.66	1.98
$\Delta E_{t_{2g}}$	0.32	0.33	0.31	0.36	0.23
$10Dq$ (eV)	1.80	1.50	1.64	1.56	1.52
D_s (eV)	0.29	0.33	0.42	0.43	0.32
D_t (eV)	0.11	0.13	0.19	0.19	0.14
Δ_{pd} (eV)	2.20	n.d.	n.d.	n.d.	n.d.
T_{pd} (eV)	3.20	n.d.	n.d.	n.d.	n.d.
T_{pp} (eV)	0.81	n.d.	n.d.	n.d.	n.d.

Figure 10. (Left panels) The effective CF parameter $10Dq$ as a function of the lattice constant: linear (lower) and logarithmic (upper panel) scale. (Right panel) The splitting of the t_{2g} and e_g states as a function of the out-of-plane nearest neighbor distance l.

structure of CuO in which they treat the d–d Coulomb and exchange interaction within full atomic multiplet theory and use symmetry-dependent Cu 3d–O 2p hybridization to describe photoelectron spectroscopic data. In the model, they consider a $(CuO_4)^{6-}$ cluster (plaquette), but
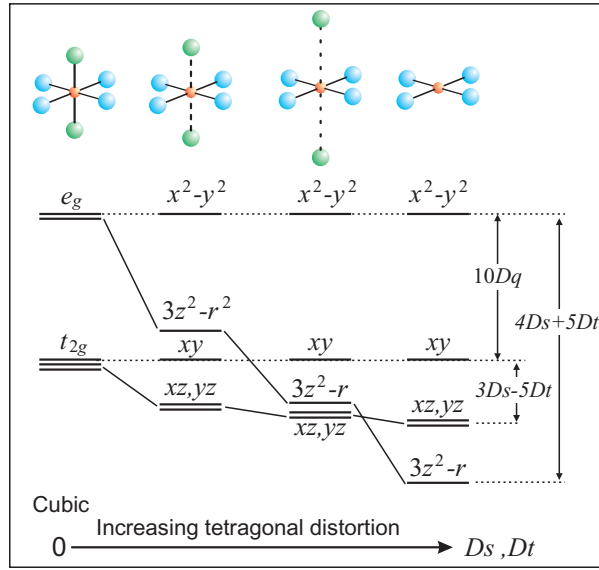
Figure 11. Local crystal field and energy level diagram for d orbitals in spherical, cubic (O_h) and tetragonal (D_{4h}) symmetry.

neglect apical oxygens. In our case, this model seems to be only partially justified: in fact, we can expect that the 2D cluster, which does not include the apical ligands, cannot fully account for the dependence of Δ_{e_g} and $\Delta_{t_{2g}}$ on the out-of-plane Cu–ligand distance l. Within this covalent picture, the energy levels of d states are written as

$$E_{x^2-y^2}^{\rm cov} = \frac{1}{2}(\Delta_{\rm pd} - T_{\rm pp}) - \sqrt{T_{\rm pd}^2 + \frac{1}{4}(\Delta_{\rm pd} - T_{\rm pp})^2}, \tag{23}$$

$$E_{3z^2-r^2}^{\rm cov} = \frac{1}{2}(\Delta_{\rm pd} + T_{\rm pp}) - \sqrt{\left(\frac{T_{\rm pd}}{\sqrt{3}}\right)^2 + \frac{1}{4}(\Delta_{\rm pd} + T_{\rm pp})^2}, \tag{24}$$

$$E_{xy}^{\rm cov} = \frac{1}{2}(\Delta_{\rm pd} + T_{\rm pp}) - \sqrt{\left(\frac{T_{\rm pd}}{2}\right)^2 + \frac{1}{4}(\Delta_{\rm pd} + T_{\rm pp})^2}, \tag{25}$$

$$E_{xz/yz}^{\rm cov} = \frac{1}{2}\Delta_{\rm pd} - \sqrt{\left(\frac{T_{\rm pd}}{2\sqrt{2}}\right)^2 + \frac{1}{4}\Delta_{\rm pd}^2} \tag{26}$$

where $\Delta_{\rm pd}$ is the CT energy, $T_{\rm pd}$ is the ground state Cu 3d–O 2p hybridization energy and $T_{\rm pp}$ is the nearest-neighbor O 2p–O 2p hybridization energy. For LCO, the values of the parameters were obtained by taking the value of $\Delta_{\rm pd}$ from independent experiments (2.2 eV [36]) and by fulfilling two of the three equations for $T_{\rm pd}$ and $T_{\rm pp}$. The values that better reproduce the experimentally determined energies of Cu-3d states in LCO are $T_{\rm pd} = 3.20$ eV and $T_{\rm pp} = 0.81$ eV. However, this 2D cluster cannot describe the energy sequence found for SCOC, CCO and NdBCO. In fact, in those compounds $E_{3z^2-r^2} > E_{xy}$, whereas $E_{3z^2-r^2}^{\rm cov} < E_{xy}^{\rm cov}$ for any value of $\Delta_{\rm pd}$, $T_{\rm pd}$ and $T_{\rm pp}$, as can be seen from the equations above. It is anyhow interesting to note that this model predicts a power law for the xy to x^2-y^2 energy splitting with exponent $n = 3.5$, dictated by the dependence of the overlap integrals on the Cu–O distance [49]. This value is rather close to the experimental one.

6. Conclusions

Using Cu L_3 RIXS we have unequivocally determined the energy of dd excitations (directly related to the energy of Cu-3d states) in several layered cuprates, parent compounds of high-T_c superconductors. These values were largely unknown until now, because other experimental techniques could provide only partial or ambiguous results. For that reason the possible role of dd excitations in superconductivity of cuprates has often been controversial. Three main outcomes can be extracted from the comparison of the quantitative results summarized in table 1.

(i) The dd excitation average energy is about 1.9 eV and, more importantly, the minimum lies above 1.4 eV. This finding resolves speculations made in the literature about a possible role of $3z^2 - r^2$ states lying as close as 0.5 eV to the $x^2 - y^2$ ground state. The absence of dd excitations in the mid-infrared spectral region greatly supports the hypothesis that magnetic excitations (up to 250–300 meV) play a major role in Cooper pairing in cuprate superconductors, as one can obtain from the solution of the Eliashberg equations [8]. However, dd excitations can still be of importance for a full description of high-T_c superconductivity [10]. In particular, the fact that $E_{3z^2-r^2}$ greatly varies from sample to sample is potentially very important in determining T_c [12].

(ii) Apical ligands do have an influence on dd excitations, but a quantitative trend cannot be predicted by simple models such as crystal field or 2D clusters. As a consequence more sophisticated calculations [55, 56] are needed in order to reproduce the energy position of 3d states in cuprates case by case, as determined experimentally.

(iii) A simple relation of the xy state energy to the in-plane lattice parameter exists. It is a power law ($E_{xy} \propto a^{-n}$) with exponent $n \simeq 4.2$, i.e. in between the prediction of the crystal field model (purely electrostatic, $n = 5$) and that of a 'covalent' model following Harrison's overlap integrals ($n = 3.5$). The dependence of overlap integrals on the interatomic distances is of great importance in cuprates [57] as it drives the super-exchange interaction too, which provides the strong antiferromagnetic background in high-T_c superconductors (nevertheless one should not forget that overlap integrals are also strongly affected by Cu–O–Cu bond angles, a variable not considered in this work). Again, although indirectly, a better knowledge of dd excitations can be of great help for a full description of superconductivity in cuprates.

In conclusion, we have made a solid assessment of the dd excitations in cuprates. These results can serve as the experimental basis for advanced calculations of these same energies. Further measurements, both on parent compounds and on superconductors, could look for correlations between the dd excitation spectrum and the superconducting properties of the cuprates.

Acknowledgments

IOP Institute of Physics Φ DEUTSCHE PHYSIKALISCHE GESELLSCHAFT

References

[1] Bennemann K H and Ketterson J B 2008 Superconductivity *Novel Superconductors* vol 2 (Berlin: Springer)
[2] Johnston S, Vernay F, Moritz B, Shen Z-X, Nagaosa N, Zaanen J and Devereaux T P 2010 *Phys. Rev.* B **82** 064513
[3] Abanov A, Chubukov A V and Schmalian J 2003 *Adv. Phys.* **52** 119
[4] Dai P, Mook H A, Hayden S M, Aeppli G, Perring T G, Hunt R D and Doğan F 1999 *Science* **284** 1344
[5] Kastner M A, Birgeneau R J, Shirane G and Endoh Y 1998 *Rev. Mod. Phys.* **70** 897
[6] Braicovich L *et al* 2010 *Phys. Rev. Lett.* **104** 077002
[7] Scalapino D J 1995 *Phys. Rep.* **250** 329
[8] Le Tacon M *et al* unpublished work
[9] Holcomb M J 1996 *Phys. Rev.* B **54** 6648
[10] Little W A, Holcomb M J, Ghiringhelli G, Braicovich L, Dallera C, Piazzalunga A, Tagliaferri A and Brookes N B 2007 *Physica* C **460–462** 40
[11] Ohta Y, Tohyama T and Maekawa S 1991 *Phys. Rev.* B **43** 2968
[12] Sakakibara H, Usui H, Kuroki K, Arita R and Aoki H 2010 *Phys. Rev. Lett.* **105** 057003
[13] Chen C T, Tjeng L H, Kwo J, Kao H L, Rudolf P, Sette F and Fleming R M 1992 *Phys. Rev. Lett.* **68** 2543
[14] Newman R and Chrenko R M 1959 *Phys. Rev.* **114** 1507
[15] Fujimori A and Minami F 1984 *Phys. Rev.* B **30** 957
[16] Fromme B, Koch Ch, Deussen R and Kisker E 1995 *Phys. Rev. Lett.* **75** 693
[17] Fromme B, Möller M, Anschütz Th, Bethke C and Kisker E 1996 *Phys. Rev. Lett.* **77** 1548
[18] Ghiringhelli G, Matsubara M, Dallera C, Fracassi F, Gusmeroli R, Piazzalunga A, Tagliaferri A, Brookes N B, Kotani A and Braicovich L 2005 *J. Phys.: Condens. Matter* **17** 5397
[19] Chiuzbaian S G, Ghiringhelli G, Dallera C, Grioni M, Amann P, Wang X, Braicovich L and Patthey L 2006 *Phys. Rev. Lett.* **95** 197402
[20] Ghiringhelli G, Piazzalunga A, Dallera C, Schmitt T, Strocov V N, Schlappa J, Patthey L, Wang X, Berger H and Grioni M 2009 *Phys. Rev. Lett.* **102** 027401
[21] Perkins J D, Graybeal J M, Kastner M A, Birgeneau R J, Falck J P and Greven M 1993 *Phys. Rev. Lett.* **71** 1621
[22] Falck J P, Perkins J D, Levy A, Kastner M A, Graybeal J M and Birgenau R J 1994 *Phys. Rev.* B **49** 6246
[23] Ghiringhelli G, Brookes N B, Annese E, Berger H, Dallera C, Grioni M, Perfetti L, Tagliaferri A and Braicovich L 2004 *Phys. Rev. Lett.* **92** 117406
[24] Lorenzana J and Sawatzky G A 1995 *Phys. Rev. Lett.* **74** 1867–70
[25] Braicovich L *et al* 2009 *Phys. Rev. Lett.* **102** 167401
[26] Salamon D, Liu D, Klein M V, Karlow M A, Cooper S L, Cheong S-W, Lee W C and Ginsberg D M 1995 *Phys. Rev.* B **51** 6617
[27] Kuiper P, Guo J-H, Såthe C, Duda L C and Nordgren J 1998 *Phys. Rev. Lett.* **80** 5204
[28] Middlemiss D S and Mackrodt W C 2008 *J. Phys.: Condens. Matter* **20** 015207
[29] Tanaka S and Kotani A 1993 *J. Phys. Soc. Japan* **62** 464
[30] Ament L J P, Ghiringhelli G, Moretti Sala M, Braicovich L and van den Brink J 2009 *Phys. Rev. Lett.* **103** 117003
[31] Guarise M *et al* 2010 *Phys. Rev. Lett.* **105** 157006
[32] Strocov V N *et al* 2010 *J. Synchrotron. Radiat.* **17** 631
[33] Ghiringhelli G *et al* 2006 *Rev. Sci. Instrum.* **77** 113108
[34] Dallera C, Puppin E, Trezzi G, Incorvaia N, Fasana A, Braicovich L, Brookes N B and Goedkoop J B 1996 *J. Synchrotron. Radiat.* **3** 231
[35] Dinardo M E, Piazzalunga A, Braicovich L, Bisogni V, Dallera C, Giarda K, Marcon M, Tagliaferri A and Ghiringhelli G 2007 *Nucl. Instrum. Methods Phys. Res.* A **570** 176
[36] Ellis D S, Hill J P, Wakimoto S, Birgeneau R J, Casa D, Gog T and Kim Y-J 2008 *Phys. Rev.* B **77** 060501

[37] Ghiringhelli G, Tjeng L H, Tanaka A, Tjernberg O, Mizokawa T, de Boer J L and Brookes N B 2002 *Phys. Rev.* B **66** 075101

[38] Salluzzo M, de Luca G M, Marrè D, Putti M, Tropeano M, Scotti di Uccio U and Vaglio R 2005 *Phys. Rev.* B **72** 134521

[39] Vaknin D, Sinha S K, Stassis C, Miler L L and Johnston D C 1990 *Phys. Rev.* B **41** 1926

[40] Qin X M, Liu Q Q, Yu Y, Yang L X, Liu J and Jin C Q 2005 *Physica* C **426–431** 510

[41] Petrykin V V, Goodlin E A, Hester J, Trofimenko E A, Kakihana M, Oleynikov N N and Tretyakov Yu D 2000 *Physica* C **340** 16–32

[42] Ghijsen J, Tjeng L H, Eskes H and Sawatzky G A 1990 *Phys. Rev.* B **42** 2268

[43] de Groot F M F, Kuiper P and Sawatzky G 1998 *Phys. Rev.* B **57** 14584

[44] van Veenendaal M 2006 *Phys. Rev. Lett.* **96** 117404

[45] Vaknin D, Sinha S K, Moncton D E, Johnston D C, Newsam J M, Safinya C R and King H E Jr 1987 *Phys. Rev. Lett.* **58** 2802

[46] Vaknin D, Caignol E, Davies P K, Fischer J E, Johnston D C and Goshorn D P 1989 *Phys. Rev.* B **39** 9122

[47] Eskes H, Tjeng L H and Sawatzky G A 1989 *Phys. Rev.* B **41** 288

[48] Kotani A 2005 *Eur. Phys. J.* B **47** 3–27

[49] Harrison W A 1980 *Electronic Structure and the Properties of Solids* (New York: Freeman)

[50] Coldea R, Hayden S M, Aeppli G, Perring T G, Frost C D, Mason T E, Cheong S-W and Fisk Z 2001 *Phys. Rev. Lett.* **86** 5377

[51] Kim Y J, Birgenau R J, Cjou F C, Erwin R W and Kastner M A 2001 *Phys. Rev. Lett.* **86** 3144

[52] Braicovich L *et al* to be published

[53] Bersuker I B 1996 *Electronic Structure and Properties of Transition Metal Compounds* (New York: Wiley)

[54] Miller L L, Wang X L, Wang S X, Stassis C and Johnston D C 1990 *Phys. Rev.* B **41** 1921

[55] Hozoi L and Laad M S 2007 *Phys. Rev. Lett.* **99** 256404

[56] Hozoi L, Siurakshina L, Fulde P and van den Brink J 2010 arXiv:1012.3603v1

[57] Di Castro D, Bianconi G, Colapietro M, Pifferi A, Saini N L, Agrestini S and Bianconi A 2000 *Eur. Phys. J.* B **18** 617